Computer Assisted Mechanics and Engineering Sciences, **2**: 289–305, 1995.

Tying algorithm for linking of finite element meshes with different degrees of refinement. Application to finite element analyses of tires

Changhong Liu, Günther Meschke, Peter Helnwein and Herbert A. Mang
Institute for Strength of Materials, Technical University of Vienna
Karlsplatz 13/202, A-1040 Vienna, Austria

(Received March 27, 1995)

A tying algorithm for the linking of two originally geometrically incompatible finite element meshes with different degrees of refinement is proposed. It is characterized by the enforcement of geometric continuity between the two meshes at their common boundary and by specification of displacement constraints for the nodes located on this boundary. The two-dimensional as well as the three-dimensional case is considered.

The proposed tying algorithm is applied to finite element analysis of the model of an automobile tire with a simplified tread profile. Consideration of this tread profile is restricted to the anticipated region of contact of the tire with the road surface and to its vicinity. For the remaining part of the analysis model a coarser finite element mesh is used. The tying algorithm is also applied to the generation of a finite element mesh with a realistic tread geometry in the aforementioned region.

1. Introduction

Numerical analyses of technical problems by means of the finite element method often involve the linking of two meshes with different degrees of refinement. One of the reasons for such a linking is the restriction of the demand for a high degree of accuracy of the solution to only a part of the investigated domain.

Several methods are available for the linking of two finite element meshes with different degrees of refinement. One of them is based on the use of transition elements [1]. The main disadvantage of this method is the formulative effort to derive such elements for a specific problem. Another method is characterized by enforcing displacement continuity at the boundary of the two meshes by means of subsidiary conditions in variational formulations [2]. These conditions can be obtained with the help either of Lagrange multipliers or of penalty terms. In general, Lagrange multiplier techniques will lead to satisfaction of the continuity condition in a weak, i.e. weighted-integral-average sense. Such techniques result in an increase of the number of degrees of freedom. This increase is equal to the number of Lagrange multipliers. Penalty techniques are *a priori* approximate. Displacement continuity at the boundary of the two meshes may also be enforced directly, i.e. without either Lagrange multipliers or penalty terms.

In this paper, such a direct tying algorithm for the linking of two originally incompatible finite element meshes with different degrees of refinement will be proposed. Figure 1 illustrates the difference between originally compatible and originally incompatible two-dimensional finite element meshes. The proposed tying algorithm is characterized by enforcing geometric compatibility between the two meshes through modification of the coordinates of nodes located on their common boundary and by specifying displacement constraints for these nodes in order to achieve geometric compatibility of the deformed configuration. For the purpose of explaining the underlying idea, the two-dimensional case will be considered first. Then, the three-dimensional case will be treated. The

proposed tying algorithm will be applied to finite element analysis of an automobile tire model with a simplified tread profile in the anticipated region of contact with a plane, rigid surface and in the vicinity of this region. Moreover, the tying algorithm will be used to generate a finite element mesh of a tire with a realistic tread geometry in the anticipated contact region and in its vicinity.

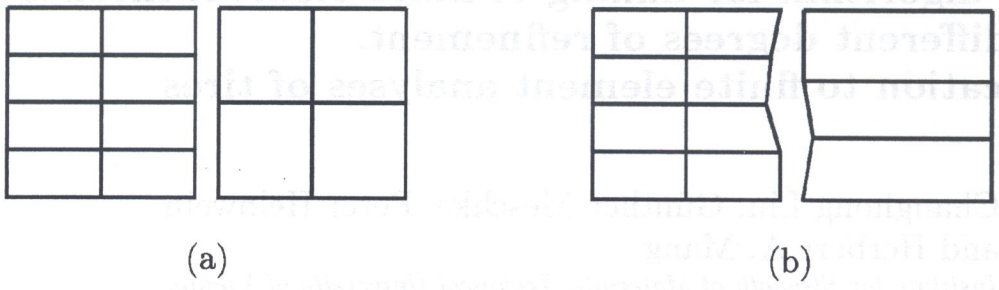

Fig. 1. Two-dimensional finite element meshes with different degrees of refinement which are to be linked; (a) originally compatible, (b) originally incompatible

2. TYING ALGORITHM FOR THE TWO-DIMENSIONAL CASE

Figure 2 shows parts of two meshes denoted as A and B. Their common boundary is referred to as Γ_A and Γ_B, respectively. Originally, Γ_A and Γ_B may be incompatible. Mesh A is finer than Mesh B. The m $[n]$ nodes on the boundary Γ_A $[\Gamma_B]$ of Mesh A $[B]$ are denoted as a_i $(i = 1, \ldots, m)$ $[b_j$ $(j = 1, \ldots, n)]$. A direct projection of the nodes a_i onto Γ_B would result in the overlapping of elements as shown in Fig. 3. Such overlaps are inadmissible.

In what follows, the procedure for linking Mesh A to Mesh B will be explained.

A2 The nodes b_1 and b_n, i.e. the first and the last node on Γ_B, are moved to the positions of the nodes a_1 and a_m, i.e. to the first and the last node on Γ_A. This is achieved by changing the coordinates of b_1 and b_n (see Figs. 4a and 4b).

B2 A search among the nodes a_i $(i = 2, \ldots, m-1)$ for the node closest to node b_j is carried out. Then b_j is moved to the position of this node by changing the coordinates of b_j. This step is carried out for $j = 2, \ldots, n-1$ (see Figs. 4b and 4c).

Note that in order to avoid a mesh with very distorted elements, the coordinates of the nodes of the coarse mesh (Mesh B) are changed in the step A2 and B2.

C2 The nodes a_i $(i = 1, \ldots, m)$, except the ones which coincide with one of the nodes b_j $(j = 1, \ldots, n)$, are projected onto the boundary Γ_B (the final position). See Figs. 4c and 4d.

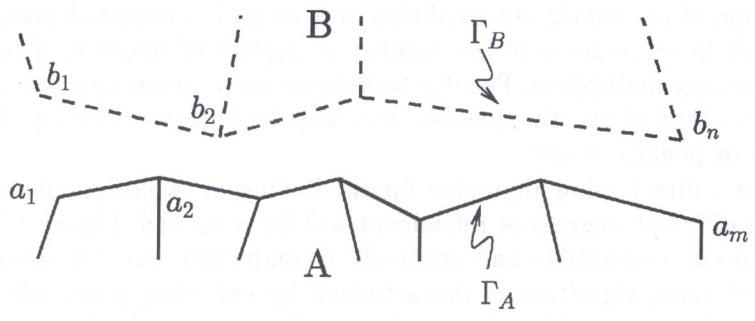

Fig. 2. Parts of two-dimensional finite element meshes with different degrees of refinement which are to be linked

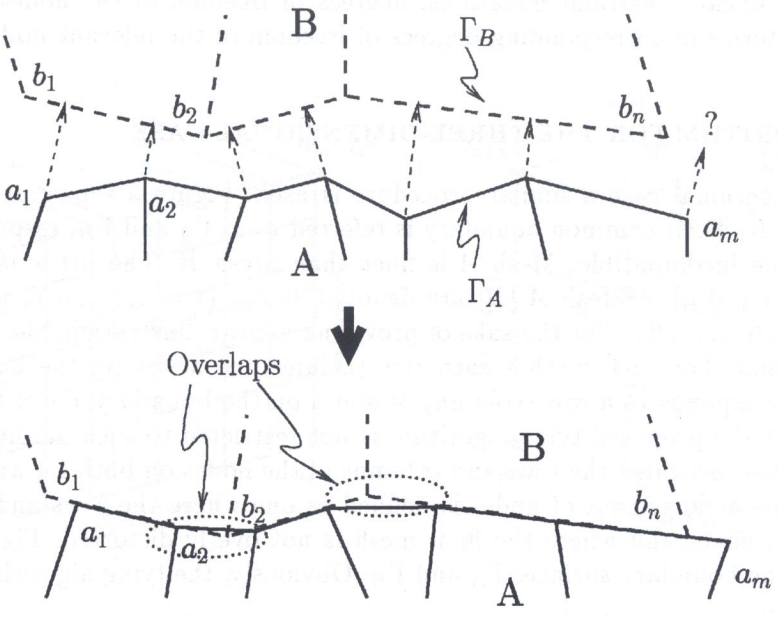

Fig. 3. Overlapping of elements caused by direct projection

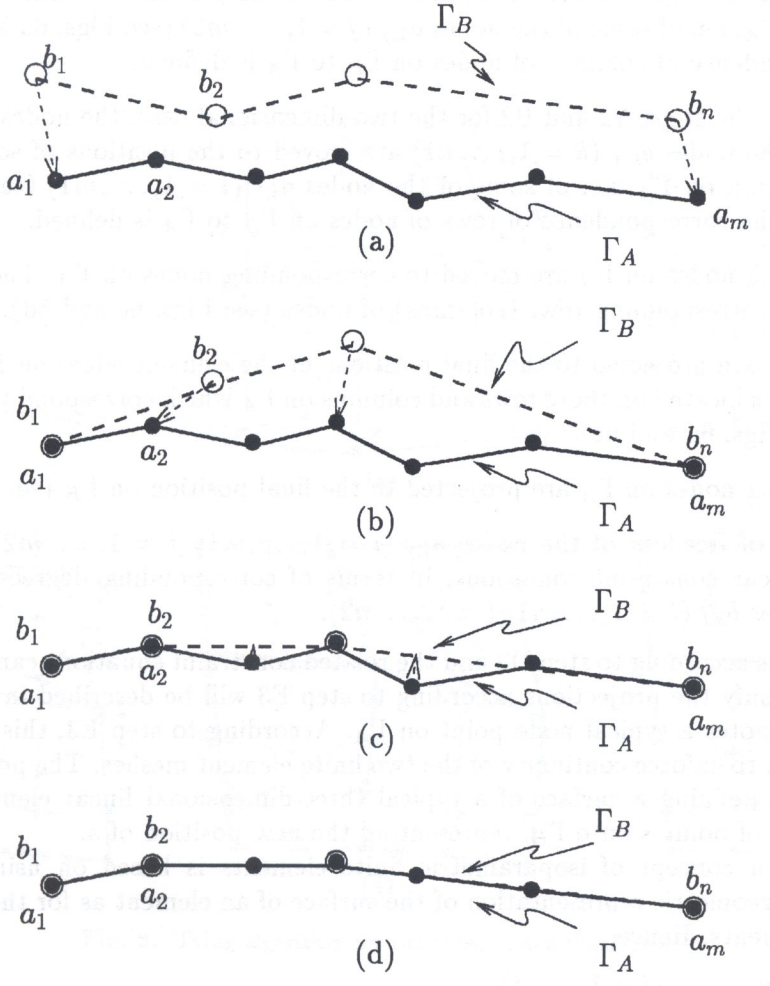

Fig. 4. Tying algorithm for the two-dimensional case

D2 By means of linear constraint equations, degrees of freedom of the nodes a_i $(i = 1, m)$ are expressed in terms of corresponding degrees of freedom of the relevant nodes b_j $(j = 1, n)$.

3. TYING ALGORITHM FOR THE THREE-DIMENSIONAL CASE

For the three-dimensional case a similar procedure is used. Figure 5 shows parts of two meshes, denoted as A and B. Their common boundary is referred to as Γ_A and Γ_B, respectively. Originally, Γ_A and Γ_B may be incompatible. Mesh A is finer than Mesh B. The $m1 \times m2$ $[n1 \times n2]$ nodes on the boundary Γ_A $[\Gamma_B]$ of Mesh A $[B]$ are denoted as $a_{i,j}$ $(i = 1, \ldots, m1;\ j = 1, \ldots, m2)$ $[b_{k,l}$ $(k = 1, \ldots, n1;\ l = 1, \ldots, n2)]$. For the sake of providing a clear illustration, the two meshes shown in Fig. 5 are regular. For such meshes each row (column) of nodes on the boundary Γ_B of the coarse mesh B corresponds to a row (column) of nodes on the boundary Γ_A of the fine mesh A. It is emphasized that the proposed tying algorithm is not restricted to such meshes. It also holds for more general meshes, provided the rows and columns of the nodes on both Γ_A and Γ_B are arranged suitably. A suitable arrangement of nodes is defined as one where the rows and the columns only follow the element edges and where the final mesh is not overly distorted. Figure 5 refers to the special case of plane boundary surfaces Γ_A and Γ_B. Obviously, the tying algorithm is not restricted to this special case.

In what follows, the procedure for the linking of Mesh A to Mesh B will be explained.

A3 Analogous to the steps A2 and B2 for the two-dimensional case, the nodes in the first row on Γ_B, i.e, the nodes $b_{1,l}$ $(l = 1, \ldots, n2)$ are moved to the positions of some of the nodes in the first row on Γ_A, i.e. of some of the nodes $a_{1,j}$ $(j = 1, \ldots, m2)$ (see Figs. 6a and 6b). Thereafter, the correspondence of columns of nodes on Γ_B to Γ_A is defined.

B3 Analogous to the steps A2 and B2 for the two-dimensional case, the nodes in the first column on Γ_B, i.e, the nodes $b_{k,1}$ $(k = 1, \ldots, n1)$ are moved to the positions of some of the nodes in the first column on Γ_A, i.e. of some of the nodes $a_{i,1}$ $(i = 1, \ldots, m1)$ (see Figs. 6b and 6c). Thereafter, the correspondence of rows of nodes on Γ_B to Γ_A is defined.

C3 The remaining nodes on Γ_B are moved to corresponding nodes on Γ_A. The correspondence is governed by corresponding rows (columns) of nodes (see Figs. 6c and 6d).

D3 Nodes on Γ_A are projected to the final positions of the element edges on Γ_B. This projection refers to nodes located on those rows and columns on Γ_A which correspond to rows and columns on Γ_B (see Figs. 6d and 6e).

E3 The remaining nodes on Γ_A are projected to the final position on Γ_B (see Figs. 6e and 7).

F3 The degrees of freedom of the nodes $a_{i,j}$ $(i = 1, \ldots, m1;\ j = 1, \ldots, m2)$ are expressed, by means of linear constraint conditions, in terms of corresponding degrees of freedom of the relevant nodes $b_{k,l}$ $(k = 1, \ldots, n1;\ l = 1, \ldots, n2)$.

The projections according to step D3 and the related constraint equations can be obtained easily. In the following, only the projections according to step E3 will be described in detail.

In Fig. 7, s denotes a typical node point on Γ_A. According to step E3, this node point will be projected onto Γ_B to enforce continuity of the two finite element meshes. The points i $(i = 1, \ldots, 4)$ are nodes on Γ_B, defining a surface of a typical three-dimensional linear element. Point c is the closest projection of point s onto Γ_B, representing the new position of s.

The well-known concept of isoparametric finite elements is based on using the same shape functions for the geometric representation of the surface of an element as for the description of the element displacements. Hence,

$$\mathbf{x}_c = N_i(\xi, \eta)\, \mathbf{x}_i \qquad (i = 1, \ldots, 4)\,, \tag{1}$$

$$\mathbf{u}_c = N_i(\xi, \eta)\, \mathbf{u}_i \qquad (i = 1, \ldots, 4)\,, \tag{2}$$

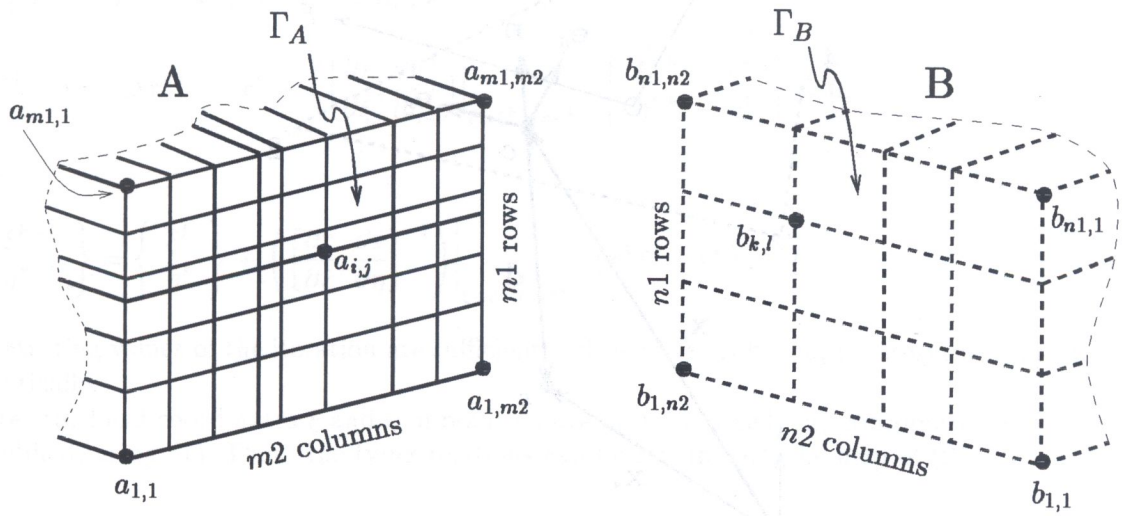

Fig. 5. Parts of three-dimensional meshes with different degrees of refinement which are to be linked

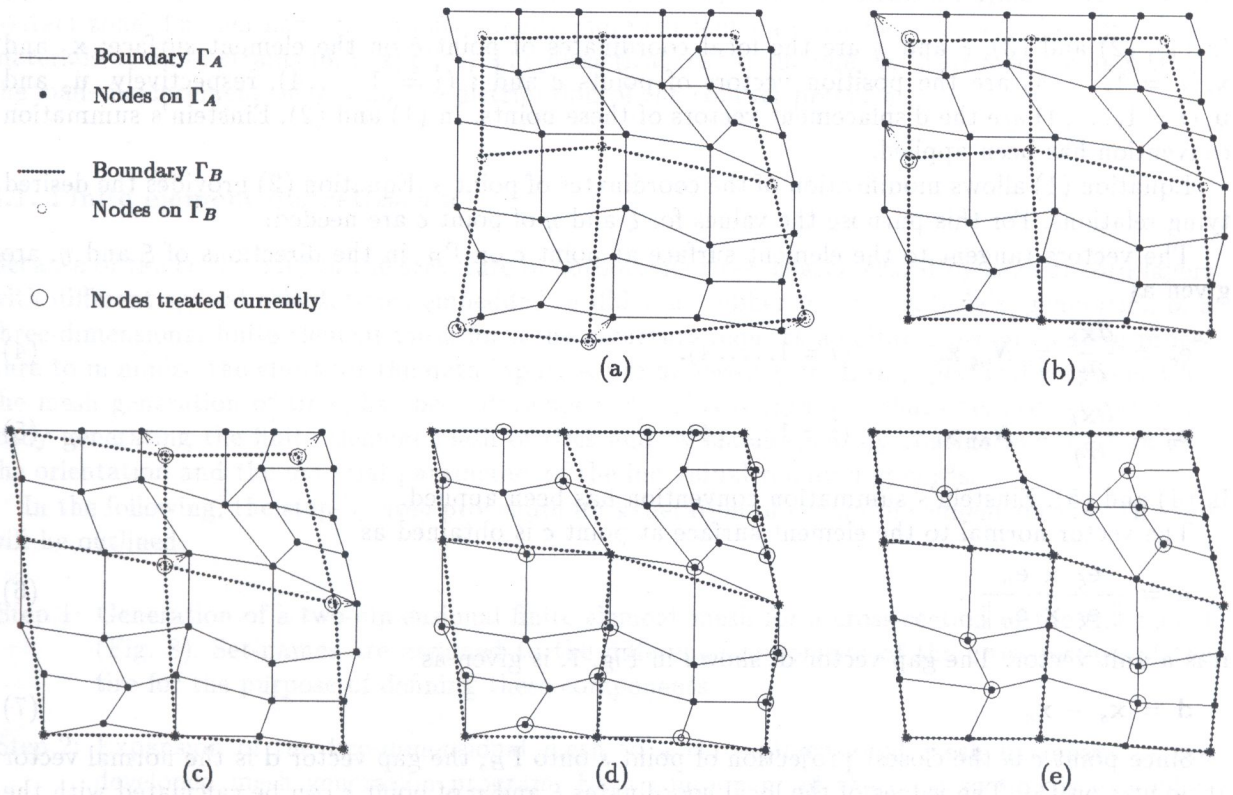

Fig. 6. Tying algorithm for the three-dimensional case

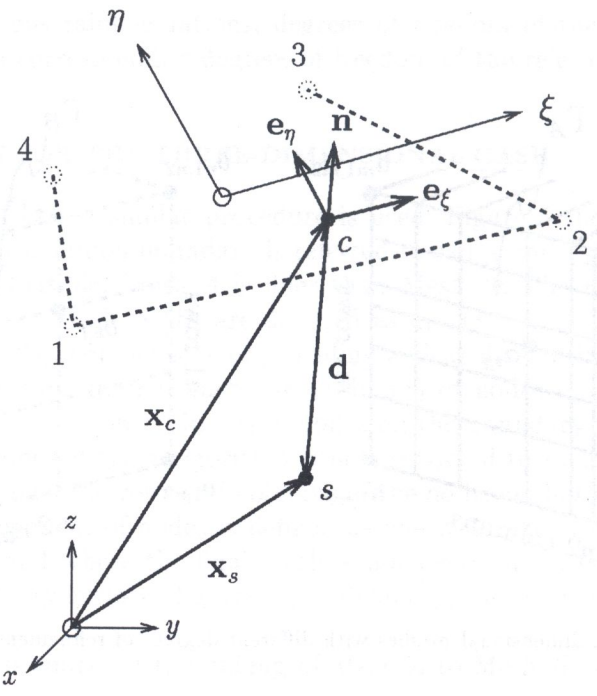

Fig. 7. Projection of node s on Γ_A onto Γ_B (step E3 of the tying algorithm for the three-dimensional case)

where N_i is a bilinear shape function given as

$$N_i = \frac{1}{4}(1+\xi\xi_i)(1+\eta\eta_i)\,. \tag{3}$$

In (1), (2) and (3), ξ and η are the local coordinates of point c on the element surface; $\mathbf{x}_c$ and $\mathbf{x}_i\,(i=1,\ldots,4)$ are the position vectors of points c and i $(i=1,\ldots,4)$, respectively. $\mathbf{u}_c$ and $\mathbf{u}_i\,(i=1,\ldots,4)$ are the displacement vectors of these points. In (1) and (2), Einstein's summation convention has been applied.

Equation (1) allows modification of the coordinates of point s. Equation (2) provides the desired tying relations. For this purpose the values for ξ and η of point c are needed.

The vectors tangent to the element surface at point c on Γ_B, in the directions of ξ and η, are given as

$$\mathbf{e}_\xi = \frac{\partial \mathbf{x}_k}{\partial \xi} = N_{i,\xi}\,\mathbf{x}_i \qquad (i=1,\ldots,4), \tag{4}$$

$$\mathbf{e}_\eta = \frac{\partial \mathbf{x}_k}{\partial \eta} = N_{i,\eta}\,\mathbf{x}_i \qquad (i=1,\ldots,4). \tag{5}$$

In (4) and (5), Einstein's summation convention has been applied.

The vector normal to the element surface at point c is obtained as

$$\mathbf{n} = \frac{\mathbf{e}_\xi \times \mathbf{e}_\eta}{\| \mathbf{e}_\xi \times \mathbf{e}_\eta \|}\,. \tag{6}$$

$\mathbf{n}$ is a unit vector. The gap vector $\mathbf{d}$, shown in Fig. 7, is given as

$$\mathbf{d} = \mathbf{x}_s - \mathbf{x}_c\,. \tag{7}$$

Since point c is the closest projection of point s onto Γ_B, the gap vector $\mathbf{d}$ is the normal vector at point c on Γ_B. The values of the local coordinates ξ and η of point c can be calculated with the help of the normality conditions:

$$\mathbf{e}_\xi \cdot \mathbf{d} = 0, \tag{8}$$

$$\mathbf{e}_\eta \cdot \mathbf{d} = 0. \tag{9}$$

The explicit solution of these equations is relatively cumbersome. Newton's method has proved to be more convenient to obtain the local coordinates of point c. Making use of the notation of $\mathbf{r} = [\mathbf{e}_\xi, \mathbf{e}_\eta]^T \cdot \mathbf{d}$ and setting $\mathbf{r}^{k+1} = \mathbf{0}$, i.e.

$$\mathbf{r}^{k+1} = \mathbf{r}^k + \Delta\mathbf{r}^{k+1} = \mathbf{r}^k + \left(\left[\frac{\partial \mathbf{r}}{\partial \xi}, \frac{\partial \mathbf{r}}{\partial \eta} \right] \right) \Big|_{\xi=\xi^k, \eta=\eta^k} \cdot \left\{ \begin{array}{c} \xi^{k+1} - \xi^k \\ \eta^{k+1} - \eta^k \end{array} \right\} = \mathbf{0}, \tag{10}$$

yields

$$\left\{ \begin{array}{c} \xi^{k+1} \\ \eta^{k+1} \end{array} \right\} = \left\{ \begin{array}{c} \xi^k \\ \eta^k \end{array} \right\} + \left(\left[\frac{\partial \mathbf{r}}{\partial \xi}, \frac{\partial \mathbf{r}}{\partial \eta} \right]^{-1} \right) \Big|_{\xi=\xi^k, \eta=\eta^k} \cdot \left(\mathbf{r}^{k+1} - \mathbf{r}^k \right). \tag{11}$$

If the starting values of the iteration are sufficiently close to the solution, the iteration will converge quadratically.

After the local coordinates ξ and η of point c have been obtained, the coordinates of node s can be modified, using (1). Then, the tying relations can be set up with the help of (2).

4. Finite element analysis of a tire model with a simplified tread profile (Model I)

In this Section the usefulness of the proposed tying algorithm for finite element analysis of an automobile tire model with a simplified tread profile is demonstrated. This tire model is referred to as Model I. In contrast to the analysis reported in [3, 4], the numerical investigation described in this Section is characterized by considering a (simplified) tread profile and accounting for friction in the contact zone. Furthermore, a computationally more efficient finite element formulation for rubber materials at finite strains [6] is applied. The numerical results include the deformed configuration, the load–displacement curve and the distribution of the contact pressure.

4.1. Finite element discretization

Because of the complexity of the structure of automobile tires, characterized by several cord layers with different spatial orientations, embedded in different rubber matrix materials, generation of a three-dimensional finite element mesh for a tire structure requires a suitable pre-processing procedure to minimize the effort for the data input. A pre-processing program, specifically designed for the mesh generation of tires, has been developed [4]. This program is characterized by automatically generating the finite element mesh of tires and by simultaneously considering the position, the orientation and the material parameters of the individual reinforcing cords.

In the following, the step-by-step procedure for generation of the finite element mesh of the tire will be outlined.

Step 1: Generation of a two-dimensional finite element mesh for a cross-section of the tire model (Fig. 8). Set-names are assigned to the different components of the cross-section of the tire for the purpose of defining these components.

Step 2: Expansion of the two-dimensional mesh to a three-dimensional mesh by means of the developed mesh generation program. Each component of the cross-section is expanded independently from the other components. The so-obtained mesh contains an opening for the refined mesh which is used for the anticipated contact region and its vicinity (Fig. 9). Simultaneously, the parameters defining the position and the orientation of the cords at each quadrature point of each finite element are calculated.

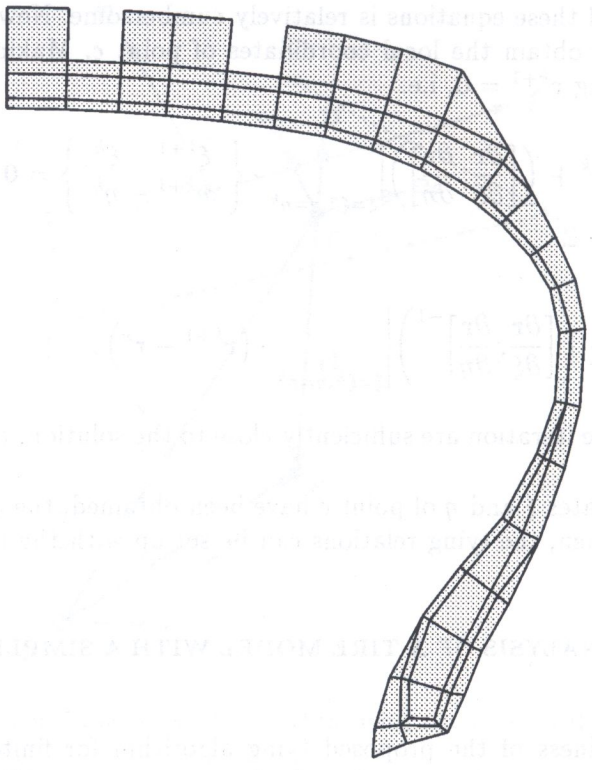

Fig. 8. Model I: Discretized cross-section of the tire model

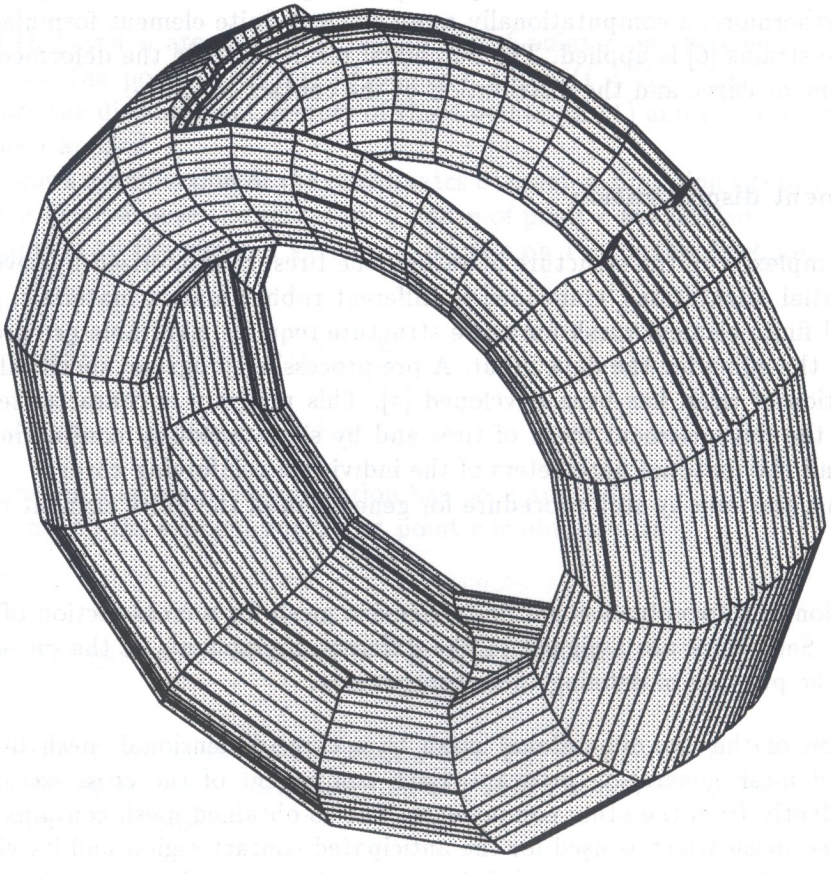

Fig. 9. Model I: Hidden-line plot of the finite element mesh of the tire model with an opening for the refined mesh

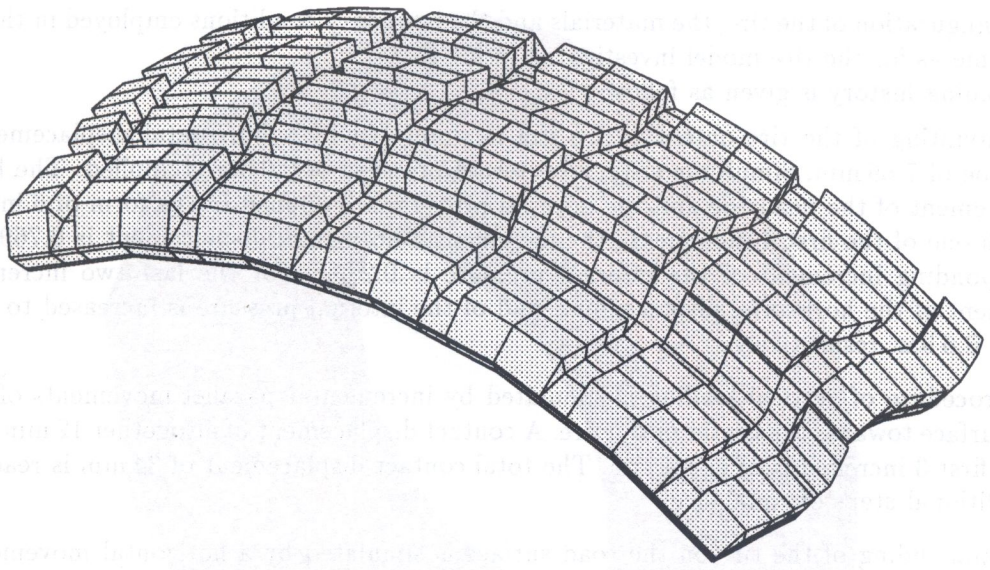

Fig. 10. Model I: Hidden-line plot of the refined finite element mesh for a part of the tire model

Step 3: Generation of the refined mesh by means of the developed mesh generation program, taking the geometry of the tread of the tire model into account. This mesh (Fig. 10) is relatively fine in order to achieve the desired degree of accuracy of the numerical solutions.

Step 4: Linking of the two finite element meshes. The proposed tying algorithm is used for enforcing continuity and specifying constraints between the two meshes with different degrees of refinement at the common boundary of the two meshes (see Fig. I).

Based on the assumption of symmetry with respect to the equatorial plane, only one half of the tire model needs to be considered for the numerical analysis. It is emphasized that this assumption is a simplification. Actually, the displacement distribution in the contact zone is characterized by central symmetry [3, 5]. However, this simplification seems to have relatively little influence on the structural stiffness and the pressure distribution [3]. The finite element mesh consists of 2544 isoparametric three-dimensional 8-node elements (1644 rubber elements, 882 elements for modelling of the cords and 18 standard isotropic elements). The purpose of the following preliminary numerical investigation is to demonstrate the usefulness of the described mesh generation procedure and of the proposed tying algorithm.

4.2. Finite element analysis

The rubber elements are based on the hybrid finite element formulation described in [6]. Compared with a finite element formulation based on the Lagrange multiplier method, the hybrid finite element formulation is more economic, both with respect to computer CPU-time and workspace [7]. A three-dimensional finite element model for cord-reinforced rubber composites, proposed by the authors [3], allows consideration of the material behaviour of such composites. It is characterized by superimposing so-called "rebar" elements as overlay-elements on corresponding three-dimensional rubber elements. The rebar elements consist of one or more layers of reinforcing cords. The material behaviour of the cords (rebar elements) is described by means of the Neo-Hookean law. This material law is formulated for the special case of a uniaxial stress state [3, 8]. The aforementioned finite element formulations were implemented, as user-defined subroutines, in the general-purpose finite element program MARC. In the numerical investigation, material and geometrical nonlinearity, "micro-buckling" of the reinforcing cords and friction between the tire and the road surface are taken into account.

The configuration of the tire, the materials and the boundary conditions employed in the analysis are the same as for the tire model investigated in [3, 4].

The loading history is given as follows:

- The mounting of the tire onto the tire rim is simulated by a horizontal displacement of the bead toe of 7.69 mm. Simultaneously, an internal pressure of 2.0 bar is applied. The horizontal displacement of the bead toe and the internal pressure are applied in the form of 6 increments. In each one of the first 4 increments the incremental horizontal displacement is 0.769 mm. The corresponding increment of the internal pressure is 0.2 bar. For the last two increments the increment of the horizontal displacement, and of the internal pressure is increased to 2.307 mm and to 0.6 bar, respectively.
- The procedure of vertical loading is simulated by incremental parallel movements of the rigid road surface towards the center of the tire. A contact displacement of altogether 12 mm is applied in the first 3 increments of equal size. The total contact displacement of 34 mm is reached after 11 additional steps of equal size.
- Frictional sliding of the tire on the road surface is simulated by a horizontal movement of the rigid road surface. Coulomb friction with a friction coefficient of $\mu = 0.3$ is used. The first displacement increment is 0.72 mm. Subsequently, 16 increments of 1 mm each are applied.

4.3. Numerical results

Figure 11 contains numerically obtained load–vertical displacement diagrams for the tire model with a simplified tread profile and for the corresponding tire model with a smooth tread [3]. The figure also shows the respective diagram resulting from an experiment of the tire model with a smooth tread [3]. The load (contact load) is defined as the integral of the contact pressure over the contact area. For the tire model with a simplified tread profile (Model I) the distribution of the contact pressure at 16 mm contact displacement (3021 N vertical load) is shown in Fig. IIa. The respective distribution at 34 mm contact displacement (6815 N vertical load) is illustrated in Fig. IIb. The deformed configuration at 34 mm contact displacement is shown in Fig. 12.

The numerically obtained contact friction force–horizontal displacement diagram is shown in Fig. 13. The distribution of the contact pressure after 15.7 *mm* of frictional sliding is illustrated in Fig. III. This distribution does not differ much from the one shown in Fig. IIb.

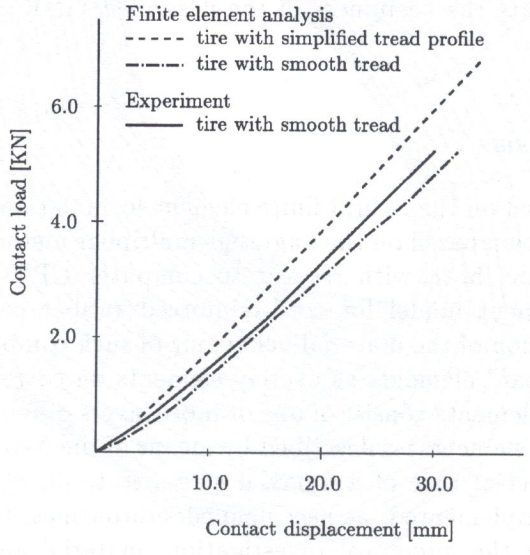

Fig. 11. Contact load — vertical displacement diagrams

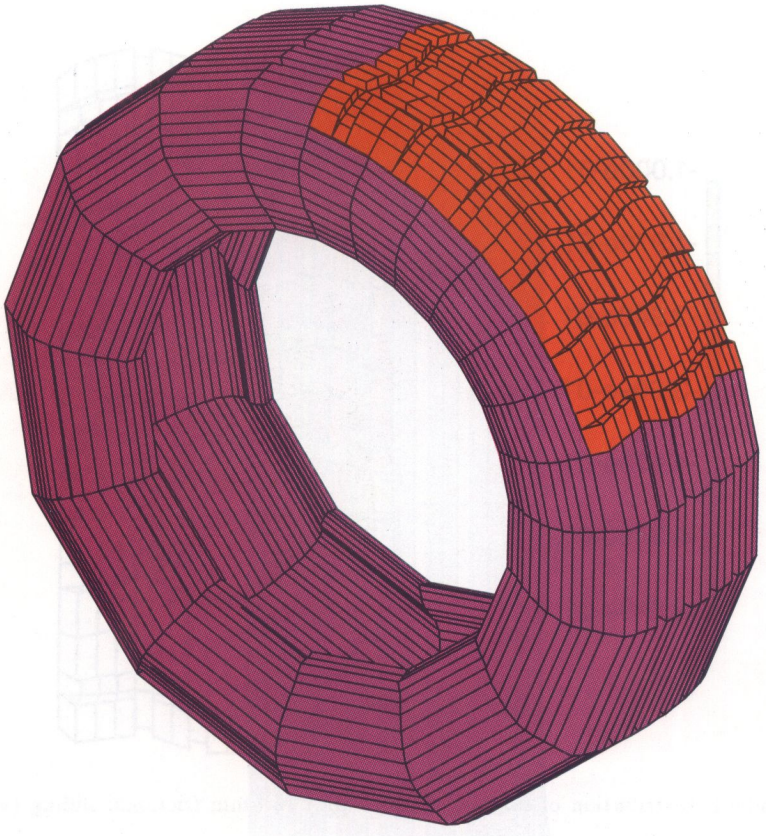

Fig. I. Model I: Hidden line plot of the finite element mesh for the model of the full tire (refined part is shown in red colour)

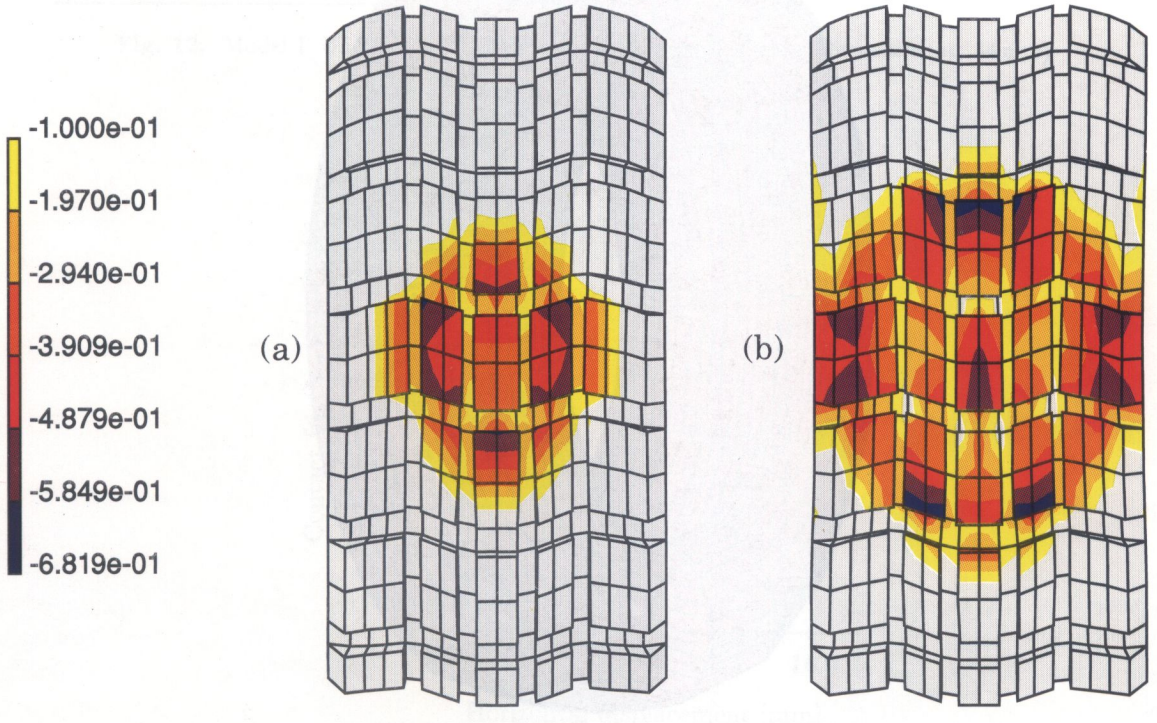

Fig. II. Model I: Distributions of contact pressure (unit: N/mm^2); (a) at 16 mm contact displacement (3021 N vertical load), (b) at 34 mm contact displacement (6815 N vertical load)

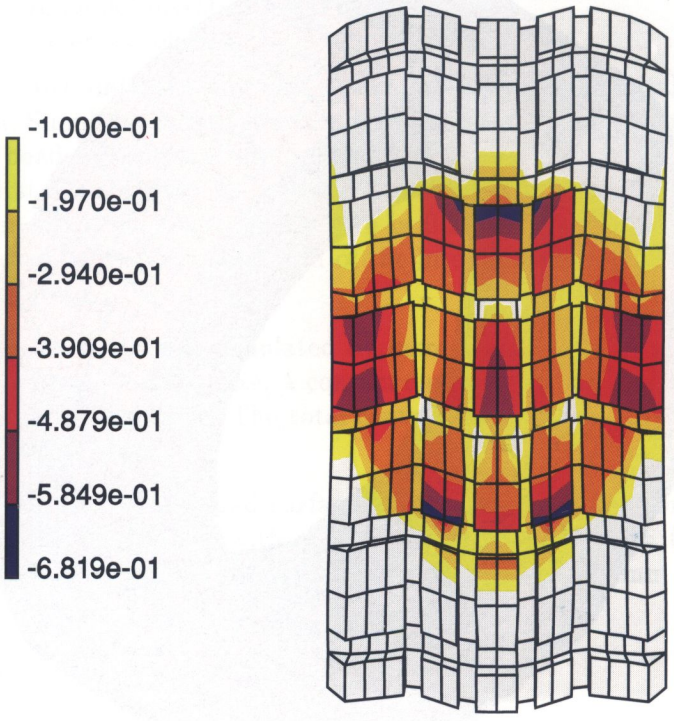

Fig. III. Model I: Distribution of contact pressure after 15.7 mm frictional sliding (unit: N/mm^2)

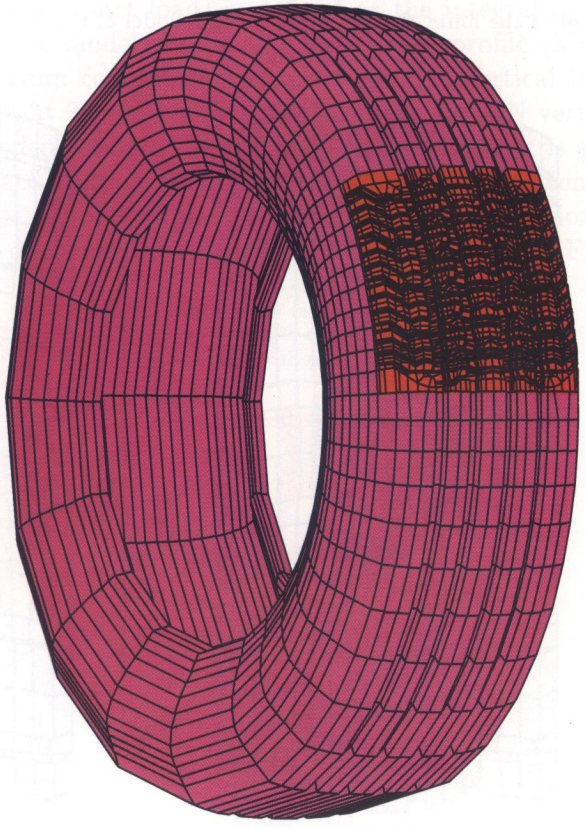

Fig. IV. Model II: Hidden-line plot of the finite element mesh for the model of the full tire (refined part is shown in red colour)

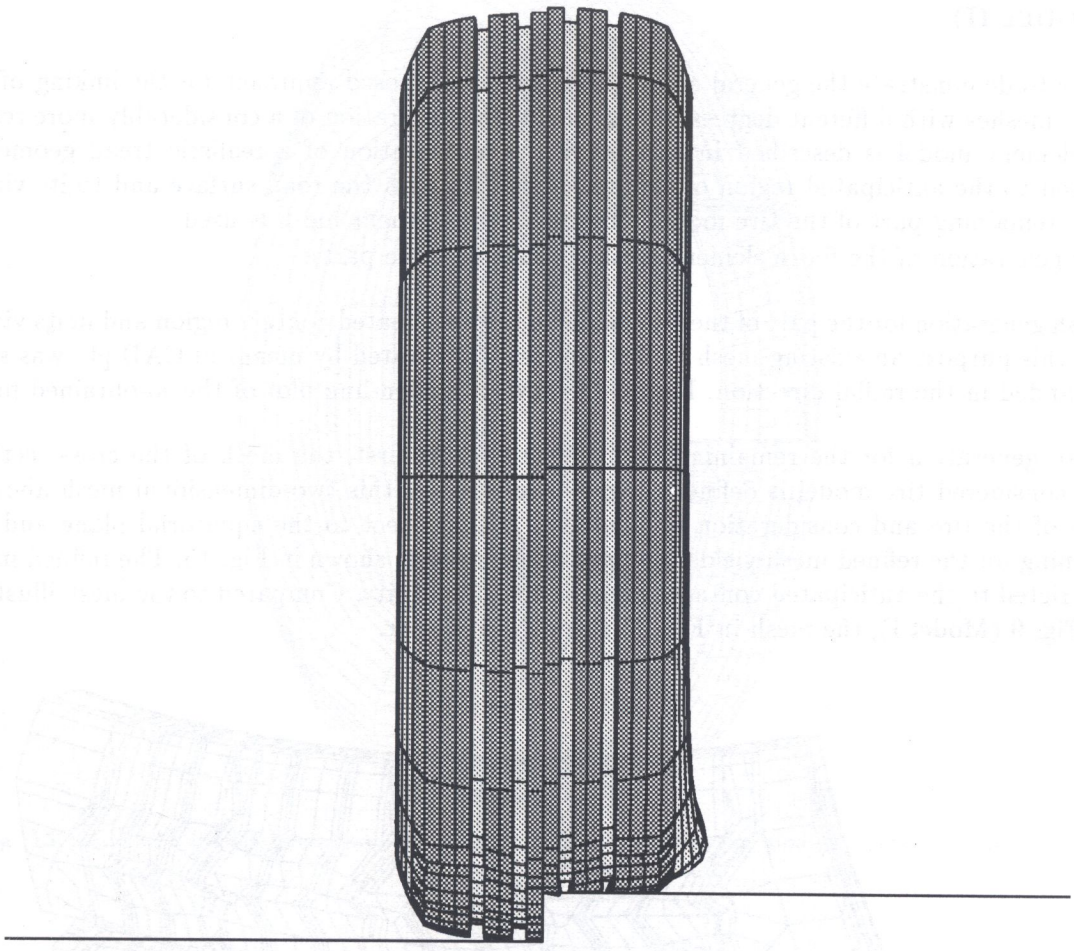

Fig. 12. Model I: Undeformed and deformed tire model (contact displacement: 34 mm)

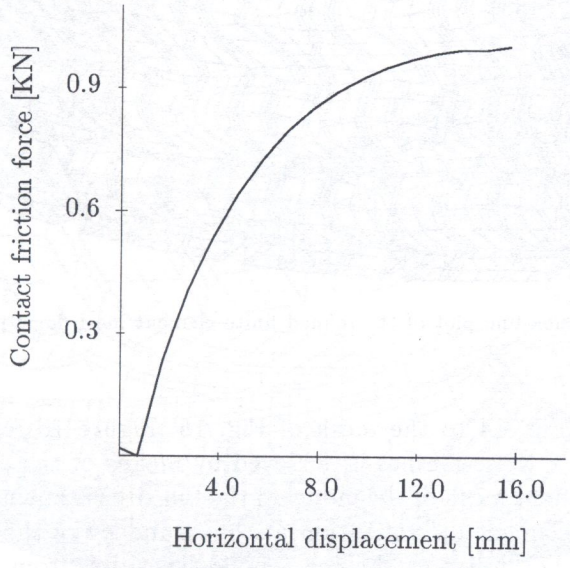

Fig. 13. Model I: Contact friction force — horizontal displacement diagram

5. Finite element mesh of a tire model with a realistic tread geometry (Model II)

In order to demonstrate the general applicability of the proposed approach for the linking of finite element meshes with different degrees of refinement, the generation of a considerably more realistic finite element model is described in this Section. Consideration of a realistic tread geometry is restricted to the anticipated region of contact of the tire with the road surface and to its vicinity. For the remaining part of the tire model a coarser finite element mesh is used.

The generation of the finite element mesh consists of three parts:

- Mesh generation for the part of the tire model in the anticipated contact region and in its vicinity. For this purpose an existing mesh of the tire tread, generated by means of CAD [4], was simply expanded in the radial direction. Figure 14 shows a hidden-line plot of the so-obtained mesh.

- Mesh generation for the remaining part of the tire. At first, the mesh of the cross-section of the considered tire model is defined (Fig. 8). Rotation of this two-dimensional mesh about the axis of the tire and consideration of symmetry with respect to the equatorial plane and of an opening for the refined mesh yields the finite element mesh shown in Fig. 15. The refined mesh is restricted to the anticipated contact region and to its vicinity. Compared to the mesh illustrated in Fig. 9 (Model I), the mesh in Fig. 15 (Model II) is finer.

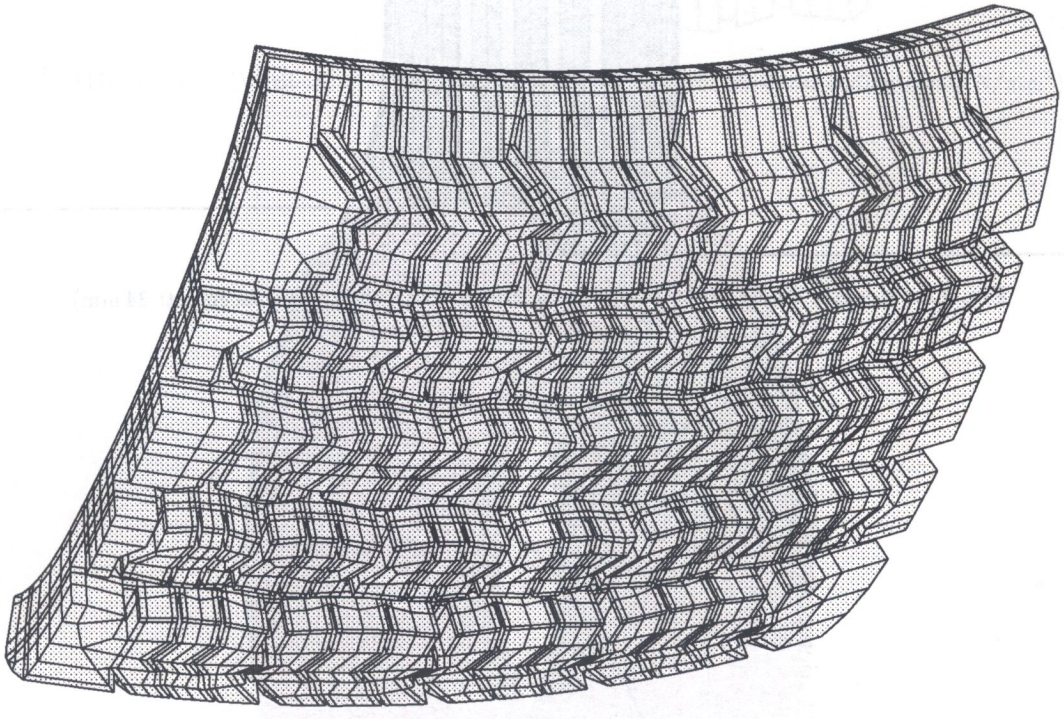

Fig. 14. Model II: Hidden-line plot of the refined finite element mesh for a part of the tire model

- Linking of the mesh of Fig. 14 to the mesh of Fig. 15. Figure 16 refers to the linking of the two meshes. Continuity of these meshes is achieved by means of the previously described tying algorithm. The finite element mesh of the model of the full tire is shown in Fig. IV. The magnified illustration of the finite element discretization at the boundary of the fine and the coarse mesh and in its vicinity (Fig. 17) indicates the continuous transition from one of these two parts of the discretization to the other one, after application of the proposed tying algorithm (Fig. 17b).

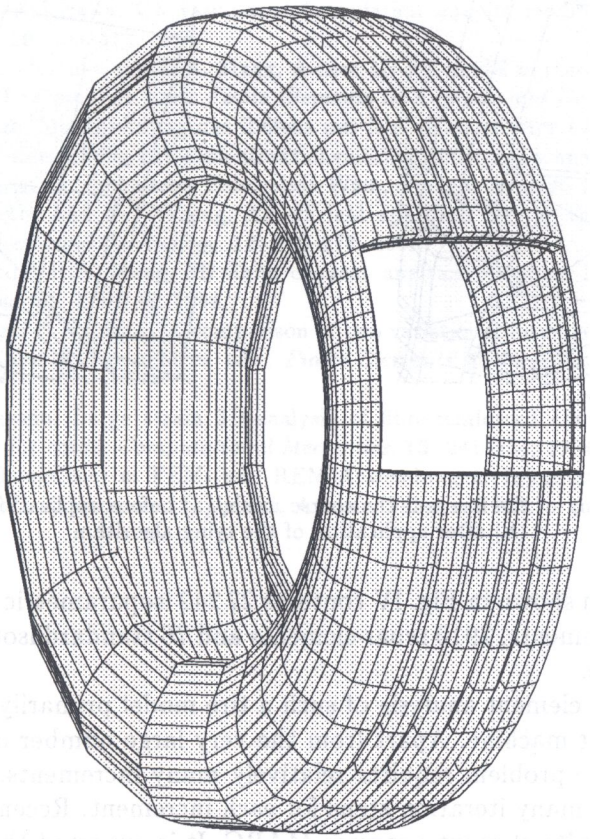

Fig. 15. Model II: Hidden-line plot of the finite element mesh of the tire model with an opening for the refined mesh

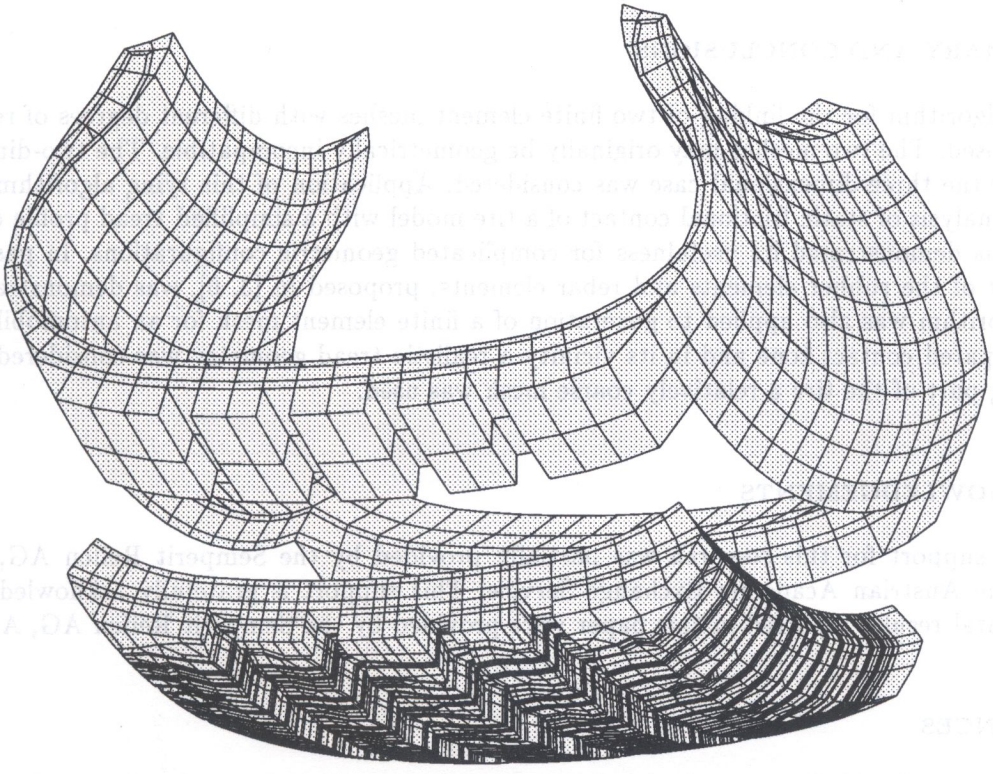

Fig. 16. Model II: Linking of the mesh of Fig. 15 to the mesh of Fig. 14

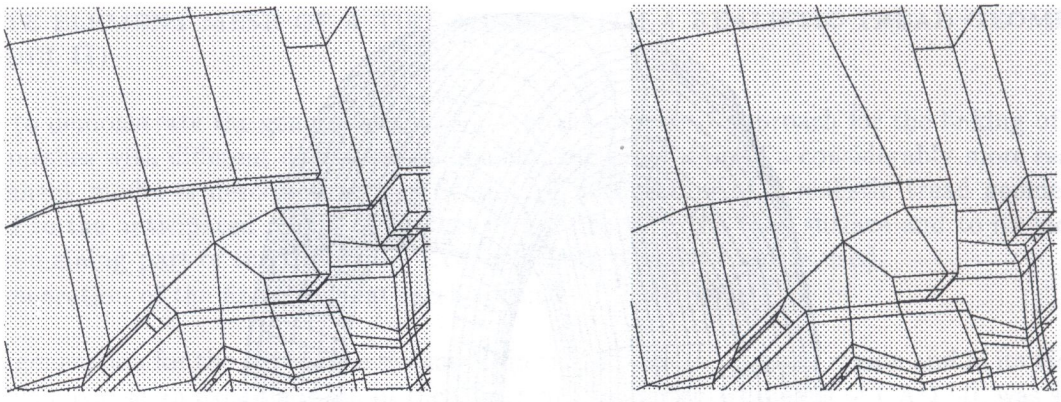

(a) (b)

Fig. 17. Model II: Linking of the fine and the coarse mesh; (a) before application of the tying algorithm, (b) after application of the tying algorithm

The finite element mesh shown in Fig. IV contains 27 242 isoparametric three-dimensional 8-node elements, 19 256 rubber elements, 7910 rebar elements and 76 standard isotropic elements. The total number of nodes is 25 695.

The feasibility of finite element analysis of such a tire model primarily depends on the capacity of the available computing machine. Apart from the very large number of degrees of freedom, the marked nonlinearity of the problem requires relatively many increments. Updating of the contact surface requires relatively many iteration steps for each increment. Recently, an iterative solver [9] was implemented in the finite element program MARC. It is expected that this solver and the use of the vector computer of the University of Technology of Vienna will render finite element analysis of the proposed tire model feasible.

6. Summary and conclusions

A tying algorithm for the linking of two finite element meshes with different degrees of refinement was proposed. The two meshes may originally be geometrically incompatible. The two-dimensional as well as the three-dimensional case was considered. Application of this tying algorithm to finite element analysis of static frictional contact of a tire model with a simplified tread profile on a rigid surface has demonstrated its usefulness for complicated geometric configurations. In passing, the suitability of the rubber elements and rebar elements, proposed in [3, 6], was demonstrated. The tying algorithm was also applied to generation of a finite element mesh for an automobile tire. In the anticipated contact zone and in its vicinity a realistic tread geometry was considered. For the remaining part of the tire a relatively coarse mesh was used.

7. Acknowledgements

Financial support for this research was partially provided by the Semperit Reifen AG, Austria, and by the Austrian Academic Exchange Service. This support is gratefully acknowledged. The experimental results reported in this paper were provided by the Semperit Reifen AG, Austria.

References

[1] C.K. Choi and Y.M. Park, An adaptive h-refinement using transition element for plate bending problems. *International Journal for Numerical Methods in Engineering.* **35**: 145–163, 1992.

[2] O.C. Zienkiewicz and S. Nakazawa, On variational formulation and its modification for numerical solution. *Computers & Structures.* **19**: 303–313, 1984.

[3] P. Helnwein, C.H. Liu, G. Meschke and H.A. Mang, A new 3D FE-model of cord-reinforced rubber composites. Application to analyses of automobile tires. *Finite Elements in Analysis and Design.* **14**: 1–16, 1993.

[4] Institut für Festigkeitslehre, Modellbildung des Reifens mit fein diskretisierter Lauffläche, Zwischenbericht über das Forschungsprojekt: Untersuchung der Reifentraktionsmechanismen auf schnee- bzw. eisbedeckten Fahrbahnen mittels FEM, Teilschritt II, Technische Universität Wien, Vienna, Austria, November 1992.

[5] J.P. Chang, K. Satyamurthy and N.T. Tseng, An efficient approach for the three-dimensional finite element analysis of tires. *Tire Science and Technology.* **16**: 249–273, 1988.

[6] C.H. Liu, G. Hofstetter and H.A. Mang, 3D finite element analysis of rubber-like materials at finite strains, *Engineering Computations.* **11**: 111–138. 1994.

[7] C.H. Liu, G. Hofstetter and H.A. Mang, A comparison of two variational formulations for rubber-like materials. In: E. Oñate, J. Periaux and A. Samuelsson, eds., *Finite Elements in the 90's*, 248–257, Springer, Barcelona, 1991.

[8] G. Meschke and P. Helnwein, Large strain 3D-analysis of fibre-reinforced composites using rebar elements: hyperelastic formulations for cords. *Computational Mechanics.* **13**: 241–254, 1994.

[9] H. Payer, Iterative Gleichungslöser in FEM- und REM-Anwendungen. Informationen des EDV-Zentrums der Technischen Universität Wien, Nummer 12, Vienna, Austria, Februar 1994.